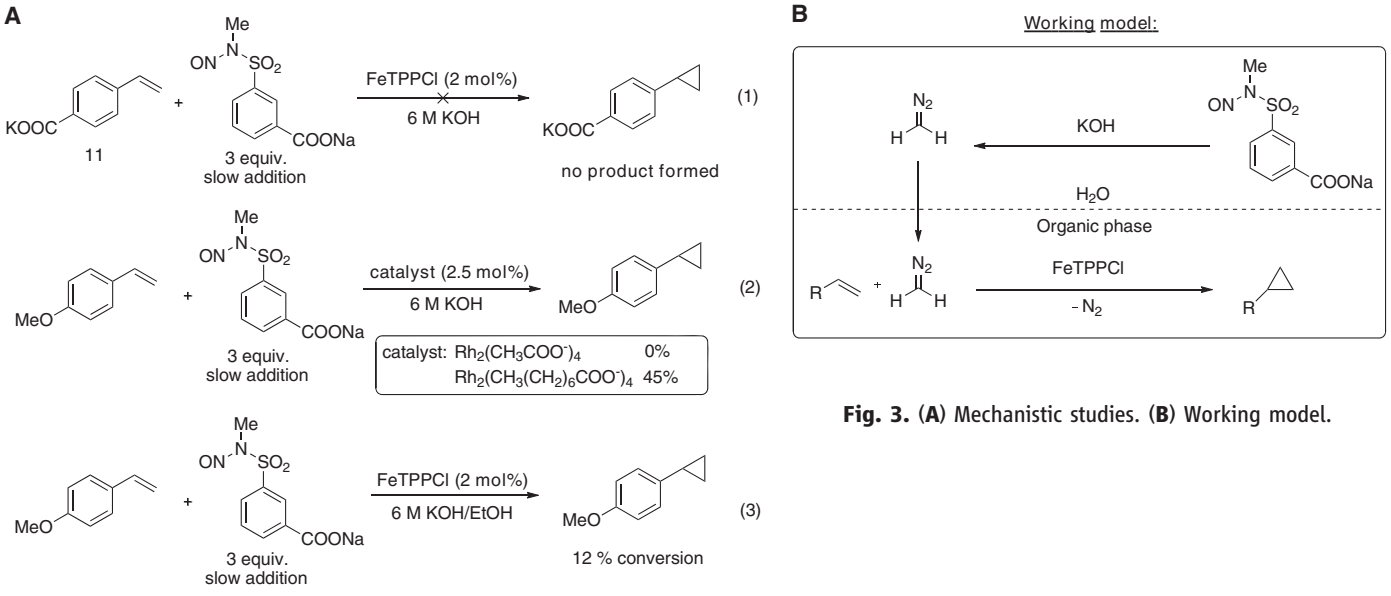

Fig. 3. (**A**) Mechanistic studies. (**B**) Working model.

4. E. B. Lewinn, *Am. J. Med. Sci.* **218**, 556 (1949).
5. T. J. de Boer, H. J. Backer, *Org. Synth. Coll.* **4**, 250 (1963).
6. H. von Pechman, *Chem. Ber.* **27**, 1888 (1894).
7. H. von Pechman, *Chem. Ber.* **28**, 855 (1895).
8. Aldrich Technical Bulletin No. AL-180 (Aldrich Chemical Company, Milwaukee, WI, 2004).
9. B. Eistert, *Angew. Chem.* **54**, 99 (1941).
10. O. M. Nefedov, Y. V. Tomilov, A. B. Kostitsyn, U. M. Dzhemilev, V. A. Dokitchev, *Mendeleev Commun.* **2**, 13 (1992).
11. In our preliminary studies, we experienced explosions when concentrated base was added to this reagent, and its use was therefore abandoned because of serious safety concerns. For a discussion about the explosive properties of *N*-nitrosomethylurea, see (*9*).
12. U.S. Department of Health and Human Services, Public Health Service, National Toxicology Program, *Report on Carcinogens* (U.S. Department of Health and Human Services, Washington, DC, ed. 12, 2011), p. 316.
13. Material Data Safety Sheet for *N*-methyl-*N*-nitroso-*p*-toluenesulfonamide (Sigma-Aldrich Chemical Company, Switzerland, 2011).
14. K.-T. Yip, D. Yang, *Chem. Asian J.* **6**, 2166 (2011).
15. R. A. Maurya, C. P. Park, J. H. Lee, D.-P. Kim, *Angew. Chem. Int. Ed.* **50**, 5952 (2011).
16. L. D. Proctor, A. J. Warr, *Org. Process Res. Dev.* **6**, 884 (2002).
17. M. Struempel, B. Ondruschka, A. Stark, *Org. Process Res. Dev.* **13**, 1014 (2009).
18. B. Morandi, E. M. Carreira, *Angew. Chem. Int. Ed.* **49**, 938 (2010).
19. B. Morandi, E. M. Carreira, *Angew. Chem. Int. Ed.* **49**, 4294 (2010).
20. B. Morandi, B. Mariampillai, E. M. Carreira, *Angew. Chem. Int. Ed.* **50**, 1101 (2011).
21. J. R. Fulton, V. K. Aggarwal, J. de Vicente, *Eur. J. Org. Chem.* **2005**, 1479 (2005).
22. R. P. Wurz, A. B. Charette, *Org. Lett.* **4**, 4531 (2002).
23. Health and Safety Executive, *Designing and Operating Safe Chemical Reaction Processes* (HSE Books, UK, 2000), p. 16.
24. D. Moody, international patent WO/2008/040947 (2008).
25. The reaction using Fe(TPP)Cl was performed with 0.5 M KOH under otherwise identical reaction conditions and afforded only 20% conversion. Strongly basic medium is thus required for the process.
26. G. Maas, *Top. Curr. Chem.* **137**, 75 (1987).
27. J. R. Wolf, C. G. Hamaker, J.-P. Djukic, T. Kodadek, L. K. Woo, *J. Am. Chem. Soc.* **117**, 9194 (1995).
28. *Iron Catalysis in Organic Synthesis, Reactions and Applications*, B. Pliekter, Ed. (Wiley-VCH, Weinheim, Germany, 2008).
29. S. Enthaler, K. Junge, M. Beller, *Angew. Chem. Int. Ed.* **47**, 3317 (2008).
30. Materials and methods are available as supporting material on *Science* Online.
31. J. Salaün, *Top. Curr. Chem.* **207**, 1 (2000).
32. M. Rubin, M. Rubina, V. Gevorgyan, *Chem. Rev.* **107**, 3117 (2007).
33. B. Morandi, J. Cheang, E. M. Carreira, *Org. Lett.* **13**, 3080 (2011).

Acknowledgments: We are grateful to Stipendienfonds der Schweizerischen Chemischen Industrie (SSCI) for a fellowship to B.M. and to ETH-Zurich for generous support through grant 0-20744-11.

Supporting Online Material

www.sciencemag.org/cgi/content/full/335/6075/1471/DC1
Materials and Methods
Figs. S1 to S16
References (*34*, *35*)

5 January 2012; accepted 14 February 2012
10.1126/science.1218781

Energy Capture from Thermolytic Solutions in Microbial Reverse-Electrodialysis Cells

Roland D. Cusick, Younggy Kim, Bruce E. Logan*

Reverse electrodialysis allows for the capture of energy from salinity gradients between salt and fresh waters, but potential applications are currently limited to coastal areas and the need for a large number of membrane pairs. Using salt solutions that could be continuously regenerated with waste heat (≥40°C) and conventional technologies would allow much wider applications of salinity-gradient power production. We used reverse electrodialysis ion-exchange membrane stacks in microbial reverse-electrodialysis cells to efficiently capture salinity-gradient energy from ammonium bicarbonate salt solutions. The maximum power density using acetate reached 5.6 watts per square meter of cathode surface area, which was five times that produced without the dialysis stack, and 3.0 ± 0.05 watts per square meter with domestic wastewater. Maximum energy recovery with acetate reached 30 ± 0.5%.

Microbial fuel cell (MFC)–based technologies are promising methods for direct electrical power production from waste organic matter, wastewater treatment, and the capture of salinity gradients in salt- and freshwater sources (*1*–*3*). Exoelectrogenic microorganisms can oxidize soluble organic matter, such as that present in wastewater (*4*, *5*), and release electrons to an electrode. Power densities with air-cathode MFCs have reached 2.7 W/m^2 by using optimized solutions with equally sized electrodes (*6*) but are lower when using complex organics or solutions (0.26 to 0.45 W/m^2) with ionic conductivities typical of domestic wastewater (~1 mS/cm) (*7*–*9*).

Reverse electrodialysis (RED) is a process for direct electricity production from salinity-gradient

Department of Civil and Environmental Engineering, 212 Sackett Building, Pennsylvania State University, University Park, PA 16802, USA.

*To whom correspondence should be addressed. E-mail: blogan@psu.edu

energy, obtained from seawater and freshwater sources, based on the use of many pairs of anion and cation exchange membranes situated between two electrodes. Many membrane pairs are needed for effective harnessing of salinity gradients as electricity, resulting in high costs for standalone RED systems (*10*, *11*). The use of natural waters in RED can result in membrane fouling without extensive pretreatment of fresh and salt water. In principle, salinity-gradient energy can be effectively captured within a microbial reverse-electrodialysis cell (MRC) by using only a small number of membrane pairs (Fig. 1). Bacterial oxidation of organic matter and oxygen reduction provide favorable electrode reactions, resulting in efficient capture of energy in the RED stack (*12*). However, RED and MRC applications are currently limited to estuarine or coastal areas because of the need for both fresh- and saltwater solutions (*12*).

Thermolytic solutions such as ammonium bicarbonate (NH_4HCO_3), which can be concentrated with low-grade thermal energy (*13*), theoretically may be able to provide the salinity-gradient energy source for a RED stack. When combined with a favorable reaction at the electrodes in an MFC, or used in a microbial electrolysis cell (MEC) for hydrogen gas production (*12*, *14*), an MRC using NH_4HCO_3 could result in more efficient capture of energy from wastewaters and other sources of biomass than could an MFC. The capture of waste heat (>40°C) energy with NH_4HCO_3 is possible with conventional and well-proven technologies, such as vacuum distillation (*15*), that can produce high-concentrate (HC) and low-concentrate (LC) salt solutions. The resulting energy difference between 1 M and 0.01 M NH_4HCO_3 HC and LC solutions is equivalent to 370 m of hydraulic head, which is even greater than that of typical ocean and river water (270 m) (*11*). NH_4HCO_3 is relatively distinct among many different chemicals that have been proposed for capturing energy through pressure differences, in a process called pressure-retarded osmosis (PRO), because of the easily volatilized ionic species (*16*). PRO requires the flow of water through specific types of membranes, distillation of larger volumes of water than would be needed for a RED stack, and mechanical conversion of pressure into electrical power. This is different than the MRC process, in which electricity is directly generated by bacteria, voltages are increased by the salinity gradient, conventional ion exchange membranes are used, and there is no direct contact of the fresh water and salt solutions.

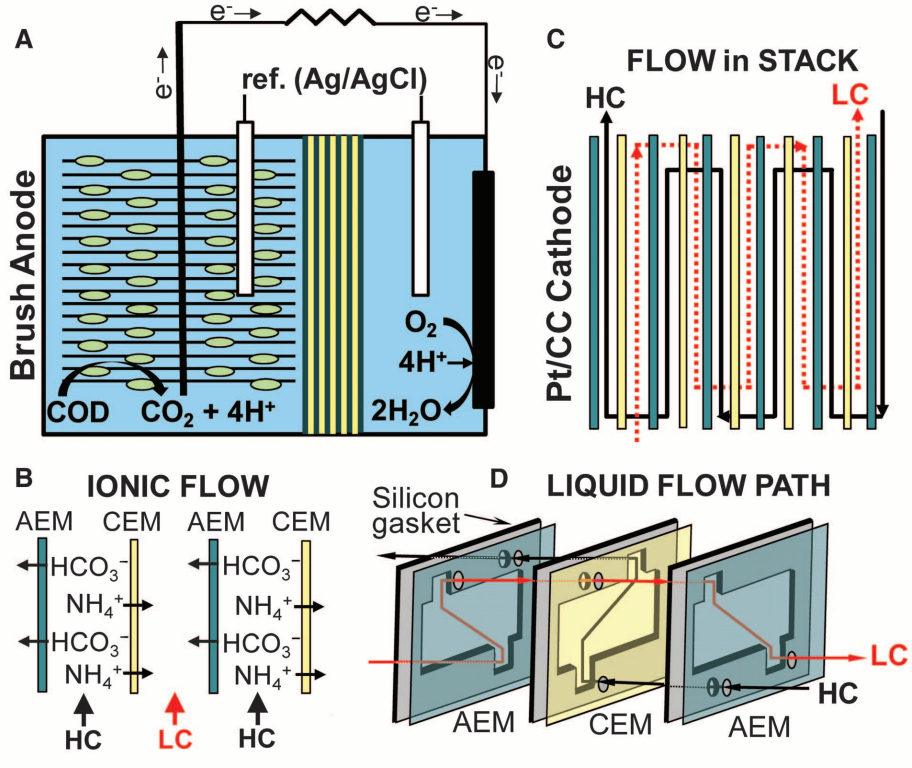

Fig. 1. (**A**) Main components of the MRC, showing the membrane stack between the electrodes, the reference electrodes, and the circuit containing a load (resistor). (**B**) Example of how the anion-exchange membranes (AEMs) and cation-exchange membranes (CEMs) are used to selectively drive the flow of positive ions to the right (toward the cathode) and the negatively charged ions to the left (toward the anode). The flow of these charged ions adds potential to the current produced by the microbes on the anode and maintains electroneutrality at the electrodes. (**C**) Expanded view of the membrane stack showing flow path of the HC and LC solutions of NH_4HCO_3. (**D**) Construction of the gaskets used to direct the flow from one LC chamber to the next LC chamber, avoiding the HC chamber through a short flow path through the membrane and gasket.

To test the utility of NH_4HCO_3 solutions for energy production, we examined four different salinity ratios (SRs) with a single HC solution (0.95 M NH_4HCO_3, conductivity of 65.5 mS/cm) in an MRC (58.4 mL) containing five membrane pairs (Fig. 1) at a fixed-solution flow rate (1.6 mL/min). The maximum power (normalized to projected cathode area of 7 cm^2) was 5.4 W/m^2 (SR = 100) with 1 g/L of sodium acetate. For these conditions, the RED stack contributed 2.1 ± 0.01 W/m^2 (39%) of the produced power, compared with 3.3 ± 0.04 W/m^2 (61%) from the oxidation of the substrate (Fig. 2A). The cell obtained peak power at a total cell voltage of 0.75 V and current density of 0.72 mA/cm^2. Lowering the flow rate (fig. S2) from 1.6 to 0.85 mL/min (4.9 ± 0.1 W/m^2) reduced power by an amount equivalent to using an SR of 50 (4.7 ± 0.1 W/m^2). The use of the RED stack and a saline catholyte alone increased power, as shown by an MRC power density of 1.7 ± 0.05 W/m^2 with membranes all containing the same saline solution (SR = 1), relative to that of a single-chamber MFC (no membranes; 1.08 ± 0.03 W/m^2). This improved performance of the MRC could be due to a number of factors, including improved charge transfer at the cathode (65.5 mS/cm), a salinity gradient between the stack and the anode, and the flow of bicarbonate ions through the anion exchange membrane, which helps to maintain anode pH at 6.9 ± 0.1 compared with a decrease in pH to 5.5 by using NaCl salt solutions (*12*).

We further examined power production using different concentrations of HC and LC solutions at a fixed salinity ratio (SR = 100). MRC power density reached a maximum of 5.6 ± 0.04 W/m^2 for the 1.1 M HC solution (Fig. 2B). This was 20% higher than that produced with an artificial seawater (NaCl) and freshwater (*12*). Internal resistances, obtained from the slope of the polarization curves (fig. S6), ranged from 170 ohms (HC = 0.5 M) to 138 ohms (HC = 1.8 M).

The most substantial impact of the RED stack on MRC performance was that it increased maximum power production using organic matter. Electrode reactions in the MRC produced up to 3.2 ± 0.2 W/m^2, which is three times the power produced in the absence of the stack in a single-chamber MFC (1.08 ± 0.03 W/m^2) (Fig. 2). The contribution of the electrodes to total power generation did not appreciably vary for HCs between 0.5 and 1.1 M (SR = 100), although power was reduced at the highest HC (1.8 M) (Fig. 2B). The use of the RED stack produced a very stable cell voltage with increasing current, with electrode potentials maintained very close to their open circuit values as current density increased (Fig. 3). In contrast, MFC electrode potentials substantially changed with increasing current. High salt concentrations (1.1 and 1.8 M) adversely affected the anode biofilm at the highest current densities, as shown by a rapid increase in the electrode potential (Fig. 3). This rapid change in electrode potential resulted in substantially reduced power densities in subsequent cycles, indicating damage

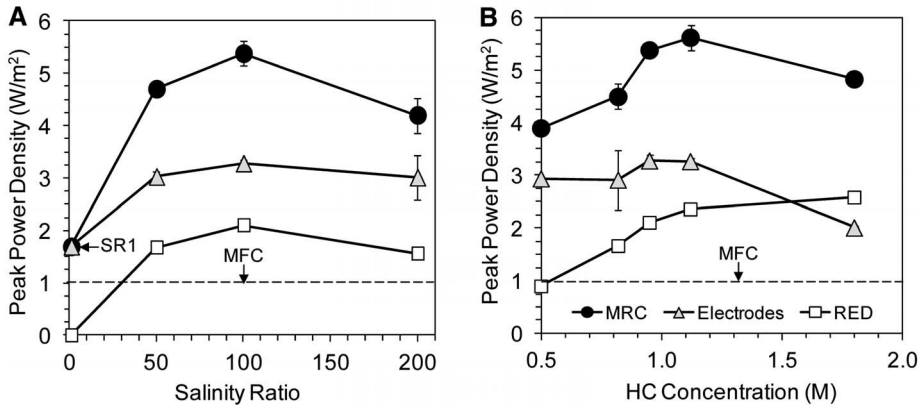

Fig. 2. Peak power densities obtained from polarization curves, apportioned to power from the RED (salinity-gradient power) compared with the electrodes (organic matter power). (**A**) Effect of SR on peak power density with a fixed HC solution (0.95 M). (**B**) Effects of HC concentrations on power with a fixed SR of 100. The dashed line represents peak power density of the same electrodes in a single chamber.

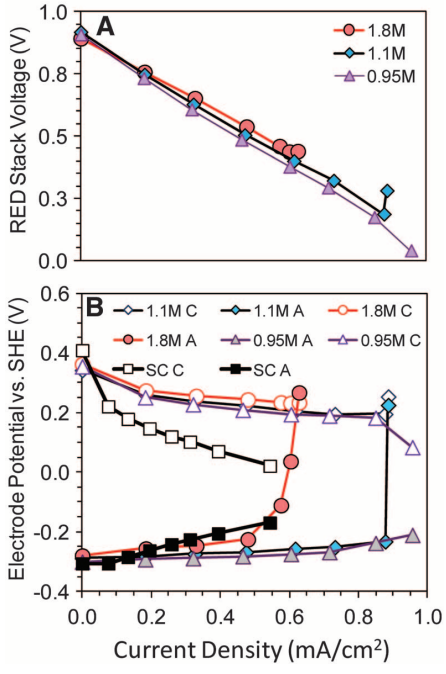

Fig. 3. (**A**) RED stack voltage and (**B**) anode (A) and cathode (C) potentials versus current density for the MRC by using different HC solutions (0.95, 1.1, and 1.8 M). The stability of the anode potential at higher current densities was the primary reason for the increased power density.

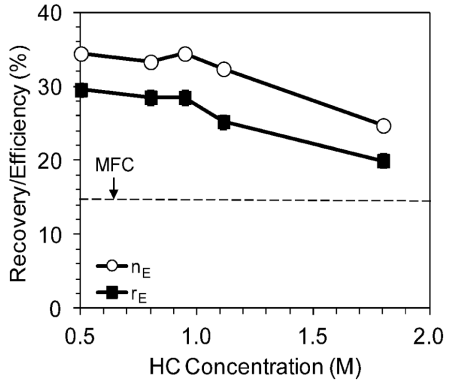

Fig. 4. Energy recovery (r_E) and energy efficiency (η_E) for the MRC in batch recycle experiments, using different HC solutions. Energy recovery is defined by the ratio of energy produced by the MRC reactor and the energy input as substrate and salinity gradient. Energy efficiency was calculated as the ratio of energy produced to the energy consumed based on the substrate used and the salinity gradient. The dashed line indicates energy recovery and efficiency using the same electrodes in a single chamber MFC reactor (no membranes).

to the anode biofilm. Several additional cycles were needed at low current densities (high resistances) to restore performance.

Energy recoveries (r_E, based on total energy entering) and energy efficiencies (η_E, energy-in minus energy going out) were higher for the MRC than a MFC. Energy recoveries for the MRC, at a fixed salinity ratio (SR = 100), ranged from 30 ± 0.5% (HC = 0.5 M) to 20 ± 0.0% (HC = 1.8 M), with energy efficiencies of 34 ± 0.5% (HC = 0.5 M) to 25 ± 0.0% (HC = 1.8 M) (Fig. 4). Maximum energy recovery in the MFC was only 14 ± 2%, with a slightly larger energy efficiency of 16 ± 2%. Coulombic efficiencies, or the percentage recovery of electrons from the substrate, were higher in the MRC (66 ± 4%) than in the MFC (35 ± 4%) because the membrane stack reduced oxygen crossover from the cathode to the anode (*12*, *17*).

The use of a salinity-gradient power source in the MRC also resulted in very high power production from domestic wastewater, with up to 2.9 ± 0.05 W/m^2 (fig. S6) produced at a HC concentration of 0.95 M (SR = 100, 1.6 mL/min flow rate). The power derived from the electrode reactions was 2.0 ± 0.05 W/m^2, which is a 740% increase in power production as compared with that achieved with wastewater in a single-chamber MFC (0.27 ± 0.05 W/m^2). This power production by the electrode reactions is 50% larger than that achieved with carbon nanotube–coated electrodes in the absence of a RED stack (*18*). Power production from wastewater dropped off after only 2 hours, indicating rapid treatment of easily degraded organic matter (fig. S7). The percentage of organic matter removal based on chemical oxygen demand (COD) was 35 ± 2%, with an energy production of 0.94 kWh/kg COD. In contrast, conventional wastewater treatment using activated sludge processes can consume 1.2 kWh/kg COD (*19*). The relatively low COD removal with wastewater, compared with essentially complete removal with acetate, is typical for biofilm processes used in wastewater treatment (*20*). Soluble COD (that passing a 0.45-μm-pore-diameter filter) can easily be removed by the biofilm in a trickling filter, for example, with particulate COD removed in a secondary solids contact process (*21*) that can be used to generate methane (*19*).

One limitation in a MRC stack arrangement with NH_4HCO_3 is nitrogen crossover from the stack into the anode chamber. The predominant nitrogen forms in the ammonium carbonate solution are ammonium (NH_4^+), ammonia (NH_3), and carbamate ($NH_4CO_3^-$). Negatively charged carbamate ions crossed the anion exchange membrane and moved into the anode chamber to balance charge (protons released by the bioanode). Total ammonia nitrogen concentrations in the anode chamber after a fed-batch cycle ranged from 263 ± 32 mg/L (HC = 0.5 M) to 590 ± 36 mg/L (HC = 1.8 M) (fig. S8). For the observed values of effluent anode pH (6.8 to 7.1), free ammonia nitrogen concentrations in the anode chamber ranged from 1.0 ± 0.2 mg/L to 2.6 ± 0.03 mg/L. Total ammonia nitrogen concentrations above 500 mg/L and free ammonia nitrogen concentrations above 11 mg/L are known to inhibit power production in MFCs (*22*). However, the main concerns of nitrogen crossover are contamination of the anode solution with ammonia and loss of the salt solution. These losses can be minimized in future designs through the use of bipolar membranes or a low-salt solution in the membrane stack nearest the anode.

The use of thermolytic solutions in RED stacks could substantially change the energy balance for wastewater treatment, enable sanitation in energy-poor areas, and allow for energy capture from renewable energy sources such as solar thermal and waste heat. Three types of wastewaters (food processing, animal, and domestic) contain nearly as much energy (17 GW) as that used for the whole water infrastructure in the United States (*23*). There is approximately nine times more energy in domestic wastewater than that required to treat it by using conventional methods (*24*). In energy-poor areas, production of electrical power from wastewater creates incentive for a community to operate a treatment plant, and therefore accomplish water sanitation. Other biomass and heat sources could also be harvested in MRCs. For example, cellulose and end products from cellulose fermentation can be used in these bioelectrochemical systems (*25*–*27*), and as much as

1.34 billion tons of biomass could be produced annually in the United States without affecting food production (*28*). Industrial applications offer a good opportunity to recover the 7 to 17% of energy used in the United States that is lost as waste heat (*29*), but solar or geothermal heat sources could also be used. All of these renewable energy sources provide opportunities for producing electricity, or alternatively hydrogen gas (*14*), from salinity gradients and biomass sources.

References and Notes

1. Intergovernmental Panel on Climate Change (IPCC), *Climate Change 2007: Synthesis Report* (IPCC, Geneva, 2007).
2. H. Liu, R. Ramnarayanan, B. E. Logan, *Environ. Sci. Technol.* **38**, 2281 (2004).
3. R. D. Cusick, P. D. Kiely, B. E. Logan, *Int. J. Hydrogen Energy* **35**, 8855 (2010).
4. B. E. Logan *et al.*, *Environ. Sci. Technol.* **40**, 5181 (2006).
5. B. E. Logan, *Nat. Rev. Microbiol.* **7**, 375 (2009).
6. Y. Fan, H. Hu, H. Liu, *Environ. Sci. Technol.* **41**, 8154 (2007).
7. Y. Ahn, B. E. Logan, *Bioresour. Technol.* **101**, 469 (2010).
8. H. Liu, B. E. Logan, *Environ. Sci. Technol.* **38**, 4040 (2004).
9. S. Cheng, H. Liu, B. E. Logan, *Environ. Sci. Technol.* **40**, 2426 (2006).
10. G. L. Wick, *Energy* **3**, 95 (1978).
11. G. Z. Ramon, B. J. Feinberg, E. M. V. Hoek, *Environ. Sci.* **4**, 4423 (2011).
12. Y. Kim, B. E. Logan, *Environ. Sci. Technol.* **45**, 5834 (2011).
13. J. R. McCutcheon, R. L. McGinnis, M. Elimelech, *Desalination* **174**, 1 (2005).
14. Y. Kim, B. E. Logan, *Proc. Natl. Acad. Sci. U.S.A.* **108**, 16176 (2011).
15. R. L. McGinnis, J. R. McCutcheon, M. Elimelech, *J. Membr. Sci.* **305**, 13 (2007).
16. T. Kim *et al.*, *Desalination* **284**, 253 (2012).
17. J. R. Kim, S. Cheng, S.-E. Oh, B. E. Logan, *Environ. Sci. Technol.* **41**, 1004 (2007).
18. X. Xie *et al.*, *Environ. Sci.* **5**, 5265 (2012).
19. P. L. McCarty, J. Bae, J. Kim, *Environ. Sci. Technol.* **45**, 7100 (2011).
20. B. E. Logan, S. W. Hermanowicz, D. S. Parker, *J. Water Pollut. Control Fed.* **59**, 1029 (1987).
21. D. Parker, J. Bratby, *J. Environ. Eng.* **127**, 380 (2001).
22. J. Y. Nam, H. W. Kim, H. S. Shin, *J. Power Sources* **195**, 6428 (2010).
23. B. E. Logan, *Environ. Sci. Technol.* **38**, 160A (2004).
24. I. Shizas, D. M. Bagley, *J. Energy Eng.* **130**, 45 (2004).
25. E. Lalaurette, S. Thammannagowda, A. Mohagheghi, P.-C. Maness, B. E. Logan, *Int. J. Hydrogen Energy* **34**, 6201 (2009).
26. F. Rezaei *et al.*, *Appl. Environ. Microbiol.* **192**, 304 (2009).
27. A. Wang *et al.*, *Bioresour. Technol.* **102**, 4137 (2011).
28. U.S. Department of Energy, Biomass as feedstock for a bioenergy and bioproducts industry: The technical feasibility of a billion-ton annual supply. *DOE/GO-102005-2135* (2005).
29. U.S. Energy Information Administration (EIA), *Annual Energy Review 2010 DOE/EIA-0384* (DOE, Washington, DC, 2010).

Acknowledgments: This research was supported by award KUS-I1-003-13 from the King Abdullah University of Science and Technology (KAUST). The data are presented in the figures and supporting online material.

Supporting Online Material

www.sciencemag.org/cgi/content/full/science.1219330/DC1
Materials and Methods
Figs. S1 to S7
References (*30*–*36*)

18 January 2012; accepted 16 February 2012
Published online 1 March 2012;
10.1126/science.1219330

Silicon Isotope Evidence Against an Enstatite Chondrite Earth

Caroline Fitoussi[1,2]* and Bernard Bourdon[1,2]

The compositions of Earth materials are strikingly similar to those of enstatite chondrite meteorites in many isotope systems. Although this suggests that Earth largely accreted from enstatite chondrites, definitive proof of this model has been lacking. By comparing the silicon (Si) isotope signatures of several extraterrestrial materials with terrestrial samples, we show that they cannot be explained by core-formation scenarios involving a bulk Earth of enstatite chondrite composition. Si isotope similarities between the bulk silicate Earth and the Moon preclude the existence of a hidden reservoir in the lower mantle, a necessary condition of the enstatite chondrite model, and require an equilibrium process after the Moon-forming impact. A three–end-member chondritic mixing model for Earth reconciles the Si isotope similarities between enstatite chondrites and Earth.

Most models of Earth's bulk composition consider that its accreting material was compositionally similar to chondritic meteorites. For example, the simplest approach for establishing Earth composition models is to consider that Earth is similar to CI carbonaceous chondrites, based on the fact that this class of meteorites is closest to the solar composition (*1*, *2*). One important issue with this approach is that, although it succeeds in matching the relative abundances of refractory lithophile elements (such as Al, Ca, and Sc), it fails to explain isotope variations. Notably, for several isotope systems such as oxygen (*3*), chromium (*4*), and nickel (*5*), the isotope composition of Earth is identical to that of enstatite chondrites. Because oxygen is a major constituent of Earth (up to 50% in mass), models that invoke a bulk Earth (a solid having the mean composition of the total Earth) of enstatite chondrite bulk composition have also been proposed (*6*, *7*). However, enstatite chondrites are undifferentiated meteorites indicating an environment more reducing than that of Earth (*8*) such that (i) the iron content is extremely small in the silicate phase and (ii) sulfides of elements that are otherwise lithophile (such as MgS or MnS) are present. Another major obstacle to an enstatite chondrite model is that the Mg/Si ratio of the upper mantle found in the most fertile peridotites (*9*, *10*) differs considerably from that of enstatite chondrites. Therefore, if the bulk Earth has a bulk enstatite chondrite composition, a correspondingly large difference of the Si abundance, which influences Mg/Si ratios, between the upper mantle and the bulk Earth must be accounted for (*11*).

Silicon isotopes, which can reveal fractionation during metal-silicate equilibrium reactions (the silicate phase gets enriched in heavy Si isotopes relative to the metal), may help resolve these discrepancies. For example, in models calling on a "solar" bulk Earth composition, Si isotopes explain how the superchondritic Mg/Si ratio of the bulk silicate Earth [(BSE), a solid having the mean composition of the terrestrial crust and mantle] resulted from the incorporation of Si into the core (*12*). If one assumes 7 weight percent (wt %) Si in the core (*2*) and metal-silicate equilibrium temperatures derived from core-formation models (*13*, *14*), the calculated δ^{30}Si value for the BSE is consistent with the measured $\delta^{30}Si_{BSE}$ (*12*). Studies using the mean of all chondrites for the bulk Earth composition also concluded that the Si isotope difference between the BSE and chondrites was due to the incorporation of Si into Earth's core (*15*, *16*). A bulk Earth with an enstatite chondrite composition (EH), however, requires a core containing 28 wt % Si, which would yield a density deficit much higher than that deduced from seismic velocities (*17*). To circumvent this issue, it was proposed that a hidden lower mantle had a higher Si content compared with the upper mantle (*7*).

To further examine the enstatite chondrite model, we analyzed the Si isotope composition of enstatite chondrites, enstatite mineral separates of enstatite chondrites and aubrites that would represent the composition of material accreting to Earth, and compared them with previously analyzed terrestrial samples and new data for lunar samples. Preparation and mass spectrometric analysis of the samples have been carried out similarly to (*12*) with only minor changes (*11*). A salient feature of this data set is that the δ^{30}Si values of enstatite chondrites are systematically lower than those of other chondrites (table S1), which confirms the suggestions from previous studies (*12*, *15*, *16*).

The Si isotope composition of the BSE (measured in terrestrial basalts and peridotites) was first reported to be $\delta^{30}Si_{BSE} = -0.38 \pm 0.04$ per mil (‰) (2 SE) (*15*). Subsequently, we measured

[1]Laboratoire de Géologie de Lyon, ENS Lyon, CNRS and Université Claude Bernard de Lyon, 46 allée d'Italie, 69364 Lyon Cedex 07, France. [2]Institute of Geochemistry and Petrology, ETH Zurich, Clausiusstrasse 25, 8092, Zurich, Switzerland.

*To whom correspondence should be addressed. E-mail: caroline.fitoussi@ens-lyon.fr